



**HAL**  
open science

# Theoretical description of ferroelectric and pyroelectric hystereses in the disordered ferroelectric-semiconductor films

A.N. Morozovka, E.A. Eliseev, Denis Remiens, S. Soyer

► **To cite this version:**

A.N. Morozovka, E.A. Eliseev, Denis Remiens, S. Soyer. Theoretical description of ferroelectric and pyroelectric hystereses in the disordered ferroelectric-semiconductor films. *Journal of Applied Physics*, 2006, 100, pp.014109-1-12. hal-00138708

**HAL Id: hal-00138708**

**<https://hal.science/hal-00138708>**

Submitted on 25 May 2022

**HAL** is a multi-disciplinary open access archive for the deposit and dissemination of scientific research documents, whether they are published or not. The documents may come from teaching and research institutions in France or abroad, or from public or private research centers.

L'archive ouverte pluridisciplinaire **HAL**, est destinée au dépôt et à la diffusion de documents scientifiques de niveau recherche, publiés ou non, émanant des établissements d'enseignement et de recherche français ou étrangers, des laboratoires publics ou privés.

# Theoretical description of ferroelectric and pyroelectric hystereses in the disordered ferroelectric-semiconductor films

Cite as: J. Appl. Phys. **100**, 014109 (2006); <https://doi.org/10.1063/1.2213172>

Submitted: 03 February 2006 • Accepted: 07 May 2006 • Published Online: 12 July 2006

A. N. Morozovska, E. A. Eliseev, D. Remiens, et al.



View Online



Export Citation

## ARTICLES YOU MAY BE INTERESTED IN

[The defect structure, sintering behavior, and dielectric responses of Cr<sub>2</sub>O<sub>3</sub>-doped Sr<sub>0.5</sub>Ba<sub>0.5</sub>Nb<sub>2</sub>O<sub>6</sub>](#)

Journal of Applied Physics **100**, 014110 (2006); <https://doi.org/10.1063/1.2213168>

[Ferroelectric thin films: Review of materials, properties, and applications](#)

Journal of Applied Physics **100**, 051606 (2006); <https://doi.org/10.1063/1.2336999>

[Ferroelectricity in undoped hafnium oxide](#)

Applied Physics Letters **106**, 232905 (2015); <https://doi.org/10.1063/1.4922272>

Lock-in Amplifiers  
up to 600 MHz



Zurich  
Instruments



# Theoretical description of ferroelectric and pyroelectric hysteresses in the disordered ferroelectric-semiconductor films

A. N. Morozovska<sup>a)</sup>

*V. Lashkaryov Institute of Semiconductor Physics, National Academy of Science of Ukraine, 41, prospect Nauki, 03028 Kiev, Ukraine*

E. A. Eliseev<sup>b)</sup>

*Institute for Problems of Materials Science, National Academy of Science of Ukraine, 3, Krjijanovskogo, 03142 Kiev, Ukraine*

D. Remiens and C. Soyer

*IEMN, UMR 8520, DOAE/MIMM, Universite de Valenciennes et du Hainaut-Cambresis, Le Mont Houy, 59313 Valenciennes Cedex 9, France*

(Received 3 February 2006; accepted 7 May 2006; published online 12 July 2006)

We have modified the Landau-Khalatnikov approach and shown that both the polar lattice and the screened charged defects determine the response of disordered ferroelectric semiconductors. This system exhibits the spatially inhomogeneous switching under the external field while the Landau-Khalatnikov model describes homogeneous switching with the sharp pyroelectric coefficient peak near the thermodynamic coercive field value. Our model gives more realistic pyroelectric hysteresis loop shape without any peaks near the coercive field and describes both qualitatively and quantitatively typical Pb(Zr, Ti)O<sub>3</sub> and (Sr, Ba)Nb<sub>2</sub>O<sub>6</sub> films pyroelectric hysteresis loops. © 2006 American Institute of Physics. [DOI: 10.1063/1.2213172]

## I. INTRODUCTION

The main peculiarity of ferroelectric materials is hysteresis of their dielectric permittivity  $\epsilon$ , displacement  $D$ , and pyroelectric coefficient  $\gamma$  over electric field  $E_0$  applied to the sample.<sup>1,2</sup> Ferroelectric  $D(E_0)$ , dielectric  $\epsilon(E_0)$ , and pyroelectric  $\gamma(E_0)$  hysteresis loops in an inhomogeneous ferroelectric-semiconductor film have several characteristic features depicted in Fig. 1(a).

In particular, ferroelectric hysteresis loops measured in PbZr<sub>x</sub>Ti<sub>1-x</sub>O<sub>3</sub> films doped with donor additives of Nb, Nd,<sup>3,4</sup> and relaxor ferroelectric films [e.g., Sr<sub>x</sub>Ba<sub>1-x</sub>Nb<sub>2</sub>O<sub>6</sub> (SBN- $x$ ), PbZr<sub>1-x</sub>Ti<sub>x</sub>O<sub>3</sub>:La (PZT:La), and PbMg<sub>1/3</sub>Nb<sub>2/3</sub>O<sub>3</sub>] have rather sloped and slim shape with low coercive fields (see, e.g., Refs. 5–8), not the square one. Aforementioned ferroelectric hysteresis loops are obtained by the conventional Sawyer-Tower method<sup>2,9,10</sup> at low frequencies of the changing applied field. In these materials low frequency dielectric hysteresis loops were obtained from the measurements of the capacity dependence on the applied voltage.<sup>11–13</sup> The loops of pyroelectric hysteresis are usually obtained by means of pyroelectric response measurements under the periodic modulation of thermal flux when applied electric field varies independently with much lower frequency.<sup>13</sup> Pyroelectric loops usually are sloped and slim; no maxima of pyroelectric response near the coercive field are observed.<sup>13,14</sup>

Nowadays such typical ferroelectric semiconductors such as BaTiO<sub>3</sub> ceramics, disordered and relaxor SBN- $x$ , PbZr<sub>x</sub>Ti<sub>1-x</sub>O<sub>3</sub> [PZT( $x/1-x$ )] solid solutions slightly doped with Fe, Cr or La, Nb, Nd, Ce, etc., their films, multilayers, and heterostructures are widely used in sensors, actuators,

electro-optic, piezoelectric, and pyroelectric devices, and memory elements.<sup>2,9,10</sup> However, the task on how to create ferroelectric material with predetermined dielectric and/or pyroelectric properties is solved mainly empirically. The correct theoretical consideration and modeling of related problems seem rather useful both for science and applications. It could answer fundamental questions about the nature of

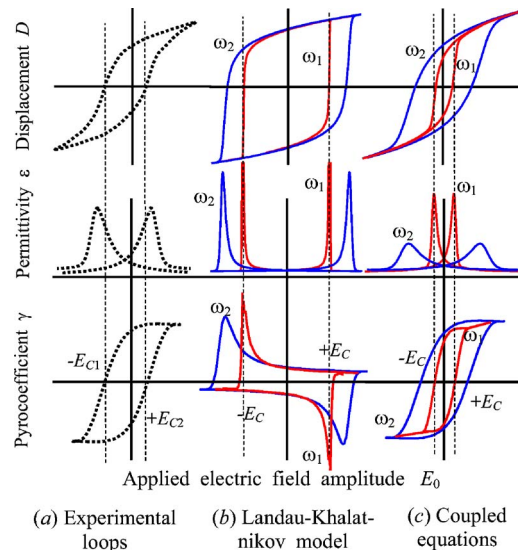


FIG. 1. Dielectric  $\epsilon(E_0)$ , ferroelectric  $D(E_0)$ , and pyroelectric  $\gamma(E_0)$  hysteresis loops. Different plots correspond to the data obtained for a semiconductor-ferroelectric film (a), the Landau-Khalatnikov model (b), and our coupled equations (c) for a bulk sample ( $\omega_1 \ll \omega_2$  are two frequencies of applied electric field). Note that the Landau-Khalatnikov thermodynamic coercive field  $E_C$  is at least several times greater than the experimentally observed values  $E_{C1}$  and  $E_{C2}$  (sometimes the loops observed in the films with thickness 50 nm–5  $\mu$ m are shifted on the value  $E_i = E_{C2} - E_{C1}$ ).

<sup>a)</sup>Electronic mail: morozo@i.com.ua

<sup>b)</sup>Electronic mail: eliseev@i.com.ua

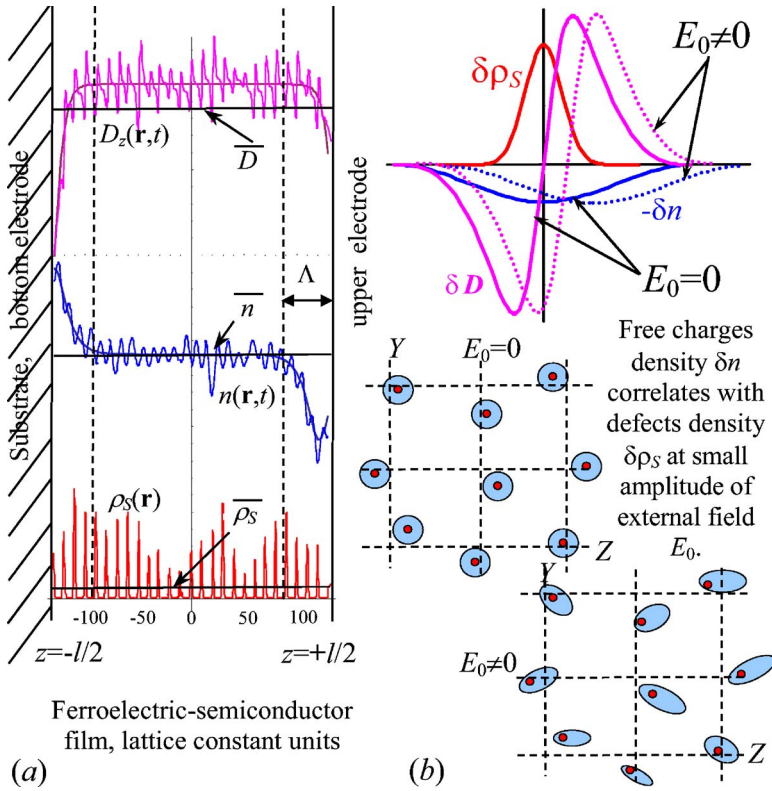


FIG. 2. Spatial distribution of displacement  $D$ , free carriers with charge density  $n$ , and sluggish defects with charged density  $\rho_S$  in an inhomogeneous ferroelectric-semiconductor film.

lattice-defect correlations and possible self-organization in the system and help tailor ferroelectric-semiconductor materials.

Conventional phenomenological approaches<sup>15,16</sup> with material parameters obtained from first-principles calculations<sup>17,18</sup> can be successfully applied to the pure ferroelectric materials,<sup>19,20</sup> but they give significantly incomplete picture of the dielectric, ferroelectric, and pyroelectric hysteresses in the doped or inhomogeneous ferroelectric semiconductors [compare Fig. 1(b) with Fig. 1(a)].

In particular, the Landau-Khalatnikov approach, which evolved for the single domain pure ferroelectric dielectrics,<sup>21,22</sup> describes homogeneous switching but presents neither domain pinning nor domain nucleation nor domain movement. The calculated values of thermodynamic coercive field<sup>1</sup> are significantly larger than its experimental values for real ferroelectrics.<sup>9,23</sup> Observed hysteresis loops usually look much thinner and sloped than the Landau-Khalatnikov ones.<sup>2,7,9,24–26</sup> Also equations of the Landau-Khalatnikov type describe homogeneous pyroelectric coefficient switching with the sharp peak near the thermodynamic coercive field value. We could not find any experiment in which the pyroelectric coefficient peak near the coercive field had been observed. Usually the pyroelectric hysteresis loops of doped ferroelectrics have typical slim shape with coercive field values much lower than the thermodynamic ones. Therefore, the modification of the Landau-Khalatnikov approach for inhomogeneous ferroelectric semiconductors seems necessary.<sup>27</sup>

In our recent papers<sup>28–32</sup> we have considered the displacement fluctuations and extrinsic conductivity caused by charged defects and thus modified the Landau-Khalatnikov approach for the inhomogeneous ferroelectric semiconduc-

tors. The derived system of three coupled equations gives the correct description of dielectric and ferroelectric hysteresis loop shapes and experimentally observed coercive field values [see Fig. 1(c)]. In this paper we evolve the proposed model<sup>29</sup> for pyroelectric response and demonstrate that the pyroelectric hysteresis loops of ferroelectric semiconductor films with charged defects could be successfully described by using six coupled equations.

## II. THEORETICAL DESCRIPTION

### A. The model and basic assumptions

The proposed model has been evolved under the following *assumptions*.

- We consider  $n$ -type ferroelectric-semiconductor film with sluggish randomly distributed impurity centers or/and growth defects. The charge density of defects  $\rho_S(\mathbf{r})$  is characterized by the positive average value  $\bar{\rho}_S$  and random fluctuations  $\delta \rho_S(\mathbf{r})$ , i.e.,  $\rho_S(\mathbf{r}) = \bar{\rho}_S + \delta \rho_S(\mathbf{r})$  [see Fig. 2(a)].
- Movable screening charge distribution  $\delta n(\mathbf{r}, t)$  with the Debye screening radius  $R_D$  surrounds each charged center [see Fig. 2(b)], so free carrier charge density  $n(\mathbf{r}, t) = \bar{n} + \delta n(\mathbf{r}, t)$  is characterized by the negative average value  $\bar{n}$  and modulation  $\delta n(\mathbf{r}, t)$ .
- Hereinafter the overbar designates the averaging of the function  $f$  over the film volume  $V$ :  $f = \bar{f} + \delta f(\mathbf{r}, t)$ . By definition  $\bar{f}(t) = (1/V) \int_V f(\mathbf{r}, t) d\mathbf{r}$  and  $\overline{\delta f(\mathbf{r}, t)} = 0$ , where  $f = \{n, \rho_S, \mathbf{E}, \mathbf{D}, \dots\}$ . The charged defects distribution is quasihomogeneous (i.e.,  $\overline{\delta \rho_S^2} = \text{const}$ ,  $\overline{(\delta \rho_S)_{x,y}} = 0$  for every  $z$  inside the film  $-l/2 \leq z \leq l/2$ ). The average distance between defects is  $d = a l^3 / N_d$  ( $a$  is the lattice

constant and  $0 < N_d \ll 1$  is defect concentration). For a micrometer-thick film with  $0.1\% \leq N_d \leq 10\%$ , one estimates that  $d \ll l$  [see Fig. 2(a)].

- The film occupies the region  $-l/2 \leq z \leq l/2$ . We suppose that the potentials of electrodes are given, so that the external field  $E_0(t)$  is applied along the polar axis  $z$ . Screening charge distribution is deformed in the external field  $E_0(t)$ , and the system “defect center  $\delta\rho_S$  + screening cloud  $\delta n$ ” causes electric field, current, and displacement fluctuations.
- The defect sluggishness means that  $|\overline{\partial\delta\rho_S(\mathbf{r})/\partial t}| \ll |\overline{\partial\delta n(\mathbf{r},t)/\partial t}|$  and  $|\overline{\partial\delta\rho_S(\mathbf{r})/\partial t}| \ll |dE_0/ldt|$ .
- The period of the changing external field is small enough for the validity of the quasistatic approximation  $\text{rot } \mathbf{E} = 0$   $\text{rot } \mathbf{H} = 0$ . Thus, Maxwell’s equations for the quasistatic inner electric field  $\mathbf{E}(\mathbf{r}, t)$  and displacement  $\mathbf{D}(\mathbf{r}, t)$  have the form:

$$\text{div } \mathbf{D} = 4\pi[\rho_S(\mathbf{r}) + n(\mathbf{r}, t)], \quad \frac{\partial \mathbf{D}}{\partial t} + 4\pi \mathbf{j}_c = 0. \quad (1)$$

Here  $\mathbf{E}(\mathbf{r}, t) \equiv \mathbf{e}_z E_0(t) + \delta\mathbf{E}(\mathbf{r}, t)$  and  $\mathbf{D}(\mathbf{r}, t) \equiv \mathbf{e}_z \overline{D}(t) + \delta\mathbf{D}(\mathbf{r}, t)$ . Maxwell’s equations (1) have to be supplemented by the material expression for macroscopic free-carrier current charge density  $\mathbf{j}_c \approx \mu n \mathbf{E} - \kappa \text{grad } n$ . One should take into account only electron mobility  $\mu$  and diffusion coefficient  $\kappa$ , allowing for the defect sluggishness. Hereinafter  $\bar{n} < 0$ ,  $\mu < 0$ , and  $\kappa > 0$ .

- We use the Landau-Khalatnikov equation for the displacement  $z$ -component relaxation as the equation of state but take into account the charged defects and correlation effects [i.e.,  $\partial^2 D_z / \partial \mathbf{r}^2 \neq 0$ , because  $D_z(\mathbf{r}, t) = D(t) + \delta D(\mathbf{r}, t)$ ]:

$$\Gamma \frac{\partial D_z}{\partial t} + \alpha D_z + \beta D_z^3 - \lambda \frac{\partial^2 D_z}{\partial \mathbf{r}^2} = E_z. \quad (2)$$

Parameter  $\Gamma > 0$  is the kinetic coefficient,  $\alpha < 0$  and  $\beta > 0$  are material parameters, and  $\lambda > 0$  is the gradient coefficient of the hypothetical pure (free of defects) uniaxial ferroelectric. For perovskites one can use the coupled Landau-Khalatnikov equations for three components  $D_{z,x,y}(\mathbf{r}, t)$  instead of one equation (2) (see, e.g., free energy in Ref. 9). Hereinafter we suppose that only the coefficient  $\alpha = -\alpha_T(T_C - T)$  essentially depends on temperature in usual form:  $\partial\alpha/\partial T = \alpha_T$ .<sup>1</sup> The temperature dependence of other coefficients  $\beta$ ,  $\lambda$ , and  $\Gamma$  could be neglected within the framework of the Landau-Ginsburg phenomenology for the second order phase transitions.<sup>1</sup> The temperature dependence  $\partial\bar{n}/\partial T$  could be neglected at temperatures  $T \gg E_a/k_B \sim 50$  K.<sup>33,34</sup>

The spatial distribution and temporal evolution of the displacement  $\mathbf{D}(\mathbf{r}, t)$  in the film are determined by the nonlinear system (1) and (2) supplemented by the initial distributions of all fluctuating variables (e.g., definite distribution of charged defects) and boundary conditions. In the Appendix we show that the system (1) and (2) is complete, because the quantities  $\delta n$  and  $\delta\mathbf{E}$  can be expressed via the fluctuations of displacement  $\delta D$  and  $\delta\rho_S(\mathbf{r})$ . The study of the do-

main wall pinning by the given distribution of charged defects and domain nucleation during spontaneous displacement reversal is beyond the scope of this paper. Therefore, hereinafter we consider only the averaged quantities. In the general case hypothetical complete exact system for average values and all their correlations could contain infinite number of differential equations and thus is not the simpler problem than the numerical solution of the stochastic differential equations.<sup>35</sup> Allowing for the aforementioned approximations and assumptions, we have no special reason to consider an exact system. Instead we propose to deal with much simpler incomplete system for the average measurable quantities  $\overline{D}$ ,  $\overline{\delta D^2}$ , etc., and to estimate/postulate some correlations such as the following.

- At small external electric field  $E_0(t)$  in comparison with microscopic one, we assume that

$$-\overline{\delta\rho_S \delta n(t)} \approx \eta(t) \overline{\delta\rho_S^2} \quad [0 \leq \eta(t, E_0) < 1], \quad (3)$$

because each charged region  $\delta\rho_S$  is surrounded by the electron density  $\delta n$  in accordance with the Debye screening mechanism, but the smooth part of charge density  $\delta n$  accommodated near the surfaces in the layer with thickness  $\Lambda$  and related to the spontaneous displacement screening does not correlate with random charged defect distribution  $\delta\rho_S$  [see Fig. 2(b), Appendix, and Ref. 29 for details].

- Taking into account that under the conditions  $d \ll l$  and  $d \ll \Lambda$  the frequency spectrum of fluctuations  $\delta D$  and  $\delta\rho_S$  has well localized maximum at spatial frequency  $2\pi/d$ , one obtains that

$$\overline{\delta D \frac{\partial^2 \delta D}{\partial \mathbf{r}^2}} \approx -\frac{1}{d^2} \overline{\delta D^2}, \quad \overline{\delta\rho_S \frac{\partial^2 \delta D}{\partial \mathbf{r}^2}} \approx -\frac{1}{d^2} \overline{\delta\rho_S \delta D}. \quad (4)$$

See Appendix and Figs. 2(a) and 3 for illustration in one-dimensional case.

## B. Coupled equations for average quantities

In our papers,<sup>29–31</sup> we modify the classical Landau-Khalatnikov equation (3) for bulk samples and obtain the system of coupled equations for average displacement  $\overline{D}$  and its mean-square fluctuation  $\overline{\delta D^2}$  and correlation with charge defect density fluctuations  $\overline{\delta D \delta\rho_S}$ . In the present paper we evolve coupled equations for a finite film with thickness  $l$  and quasihomogeneous distribution of charged defects (see Appendix for details).

The average pyroelectric coefficient  $\bar{\gamma}$  can be easily obtained by the differentiation of the coupled system<sup>29</sup> on the temperature  $T$ . In this way we obtained coupled equations for the average displacement  $\overline{D}$ , its mean-square fluctuation  $\overline{\delta D^2}$  and correlation  $\overline{\delta D \delta\rho_S}$ , pyroelectric coefficient  $\bar{\gamma} = \partial\overline{D}/\partial T$ , and its correlations with displacement fluctuations  $\overline{\delta\gamma \delta D} = \overline{\delta D \partial\delta D/\partial T}$  and charge defect density fluctuations  $\overline{\delta\gamma \delta\rho_S} = \overline{\partial\delta D \delta\rho_S/\partial T}$ :

$$\Gamma \frac{\partial \overline{D}}{\partial t} + (\alpha + 3\beta \overline{\delta D^2}) \overline{D} + \beta \overline{D}^3 = E_0(t) + E_i(l, t), \quad (5)$$

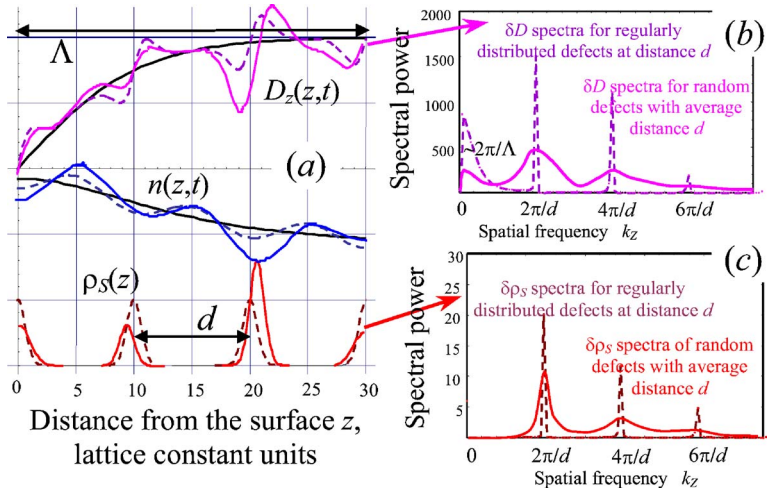


FIG. 3. 1D spatial distribution and frequency spectrum of  $\delta D(z,t)$  and  $\delta \rho_S(z)$  calculated for average distance between defects  $d=10$ , screening layer thickness  $\Lambda=30$ , film thickness  $l \approx 260$ , lattice constants, and charged defect linear concentration  $\sim 10\%$ . Dashed peaks correspond to the model 1D spectrum when identical defects are regularly distributed with distance  $d$  between them (see dashed curves). Solid curves are computer simulation of the spectrum with random defects with average distance  $d$  between them. Note that  $\delta D(z,t)$  low frequency peak with half-width  $\sim 2\pi/\Lambda$  corresponds to the smooth displacement variation in the screening layer with thickness  $\Lambda$ .

$$\begin{aligned} & \frac{\Gamma_R}{2} \frac{\partial \overline{\delta D^2}}{\partial t} + (\alpha_R + 3\beta \overline{\delta D^2}) \overline{\delta D^2} + \beta (\overline{\delta D^2})^2 \\ & = E_0(t) \left( \frac{\overline{\delta D \delta \rho_S}}{\bar{n}} - \delta E_i \right) + \frac{4\pi k_B T}{\bar{n}e} \overline{\delta \rho_S (\delta \rho_S + \delta n)}, \quad (6) \end{aligned}$$

$$\begin{aligned} & \Gamma_R \frac{\partial \overline{\delta D \delta \rho_S}}{\partial t} + (\alpha_R + 3\beta \overline{\delta D^2} + \beta \overline{\delta D^2}) \overline{\delta D \delta \rho_S} \\ & = -E_0(t) \frac{\overline{\delta \rho_S \delta n}}{\bar{n}}, \quad (7) \end{aligned}$$

$$\Gamma \frac{\partial \overline{\gamma}}{\partial t} + (\alpha + 3\beta \overline{\delta D^2} + 3\beta \overline{\delta D^2}) \overline{\gamma} = -(\alpha_T + 3\beta \overline{\delta \gamma^2}) \overline{\gamma}, \quad (8)$$

$$\begin{aligned} & \Gamma_R \frac{\partial \overline{\delta \gamma \delta D}}{\partial t} + 2(\alpha_R + 2\beta \overline{\delta D^2} + 3\beta \overline{\delta D^2}) \overline{\delta \gamma \delta D} \\ & = \left[ E_0(t) \frac{\overline{\delta \gamma \delta \rho_S}}{\bar{n}} - (\alpha_{RT} + 6\beta \overline{\delta \gamma}) \overline{\delta D^2} \right. \\ & \quad \left. + \frac{4\pi k_B T}{\bar{n}e} \overline{\delta \rho_S (\delta \rho_S + \delta n)} \right], \quad (9) \end{aligned}$$

$$\begin{aligned} & \Gamma_R \frac{\partial \overline{\delta \gamma \delta \rho_S}}{\partial t} + (\alpha_R + \beta \overline{\delta D^2} + 3\beta \overline{\delta D^2}) \overline{\delta \gamma \delta \rho_S} \\ & = -(\alpha_{RT} + 2\beta \overline{\delta \gamma \delta D} + 6\beta \overline{\delta \gamma}) \overline{\delta D \delta \rho_S}. \quad (10) \end{aligned}$$

The built-in electric field  $E_i(l,t) = (4\pi\lambda/l)(\overline{\delta n})_{x,x}|_{-l/2}^{+l/2}$  in (5) and its deviation  $\delta E_i = (2\pi/l\bar{n})[\int_{z_0}^z dz(\delta n + \delta \rho_S)]_{x,y}|_{-l/2}^{+l/2}$  in (6) are inversely proportional to the film thickness  $l$ ; thus they vanish in the bulk material.<sup>29</sup> For a finite film built-in field  $E_i(l,t)$  is induced by the smooth part of space charges  $\delta n$  accommodated near the nonequivalent boundaries  $z = \pm l/2$  (e.g., near the substrate with bottom electrode and free surface with upper electrode depicted in Fig. 3). Such layers are created by the screening carriers.<sup>15,18</sup> Built-in field value completely determines the horizontal shift of hysteresis loops observed in the ferroelectric films with thickness from dozen of nanometers up to several microns.<sup>36,37</sup> It is known that built-in field diffuses paraelectric-ferroelectric phase transition, in particular, it shifts and smears dielectric permittivity

temperature maximum.<sup>1</sup> Thus the film thickness decrease leads to the degradation of their ferroelectric and dielectric properties<sup>27</sup> up to the appearance of relaxor features.<sup>38</sup>

Bratkovsky and Levanyuk<sup>20</sup> predicted the existence of built-in field in a finite ferroelectric film within the framework of phenomenological consideration. The field had a rather general nature. Our statistical approach confirms their assumption and gives the possible expression of the field existing in the inhomogeneous ferroelectric-semiconductor film. Another partial case, when the inner electric field is induced by the film-substrate misfit strain, has been considered in the paper.<sup>39</sup>

The renormalization  $\Gamma_R \equiv \Gamma + \tau_m$  of the Khalatnikov kinetic coefficient in (6), (7), (9), and (10) is connected with the free-carrier relaxation with characteristic time  $\tau_m = 1/8\pi\mu\bar{n}$ . The renormalization of coefficients  $\alpha_R \equiv \alpha + (\lambda + k_B T/4\pi\bar{n}e)/d^2$  and  $\alpha_{RT} \equiv \alpha_T + k_B/4\pi\bar{n}ed^2$  are caused by correlation and screening effects [see (4), Appendix, and Ref. 30]. The coefficient  $\alpha = -\alpha_T(T_C - T)$  is negative in the perfect ferroelectric phase without defects ( $\delta \rho_S^2 = 0$ ,  $T_C > T$ ). For the partially disordered ferroelectric with random defects ( $\delta \rho_S^2 > 0$ ), coefficient  $\alpha_R$  is positive; moreover,  $\alpha_R \gg |\alpha|$ ,  $\alpha_{RT} \gg \alpha_T$ , and usually the ratio  $\xi = -\alpha_R/\alpha \gg 1$ .<sup>29</sup> For example, for Pb(Zr,Ti)O<sub>3</sub> solid solution,  $\alpha \sim -(0.4-2) \times 10^{-2}$ ,<sup>9</sup> gradient term  $\lambda \approx 5 \times 10^{-16}$  cm<sup>2</sup>, screening radius  $R_D \sim (10^{-6}-10^{-4})$  cm,<sup>15</sup> average distance between defects  $d \sim (10^{-6}-10^{-4})$  cm, and thus  $\alpha_R \approx k_B T/4\pi\bar{n}ed^2 \sim 10^2$ . The source of fluctuations  $\delta \rho_S(\delta \rho_S + \delta n)$  in (6) and (9) originates from the correlation between diffusion current and displacement fluctuations [see (A19) in Appendix].

Let us introduce the following dimensionless variables in the system (5)–(10):  $D_m = \overline{\delta D}/D_S$  disorder parameter  $\Delta_m = \overline{\delta D^2}/D_S^2$ ,  $K_m = -\overline{\delta D \delta \rho_S}/D_S \bar{n}$ ,  $\gamma_m = \overline{\gamma}/\gamma_S$ ,  $\Pi_m = \overline{\delta \gamma \delta D}/D_S \gamma_S$ , and  $M_m = -\overline{\delta \gamma \delta \rho_S}/\gamma_S \bar{n}$ , where  $D_S(T) = \sqrt{-\alpha(T)}/\beta$  is bulk spontaneous displacement and  $\gamma_S = dD_S(T)/dT$  is bulk pyroelectric coefficient. Note that  $\bar{n} = -\bar{\rho}_s$  allowing for the sample electroneutrality. Dimensionless system (5)–(10) acquires the form

$$\frac{\partial D_m}{\partial \tau} + (-1 + 3\Delta_m)D_m + \beta D_m^3 = E_e(\tau) + E_m(l), \quad (11)$$

$$\frac{\tau_R}{2} \frac{\partial \Delta_m}{\partial \tau} + (\xi + 3D_m^2) \Delta_m + \Delta_m^2 = -E_e(\tau) [K_m + \delta E_m(l)] + gR^2, \quad (12)$$

$$\tau_R \frac{\partial K_m}{\partial \tau} + (\xi + 3D_m^2 + \Delta_m) K_m = -E_0(\tau) R^2, \quad (13)$$

$$\frac{\partial \gamma_m}{\partial \tau} + (-1 + 3\Delta_m + 3D_m^2) \gamma_m = -(1 + 3\Pi_m) D_m^2, \quad (14)$$

$$\begin{aligned} \tau_R \frac{\partial \Pi_m}{\partial \tau} + 2(\xi + 2\Delta_m + 3D_m^2) \Pi_m \\ = \left\{ -E_e(\tau) M_m - \left[ \xi \left( \frac{T_C}{T} - 1 \right) + 6D_m \gamma_m \right] \Delta_m \right. \\ \left. + g \left( \frac{T_C}{T} - 1 \right) R^2 \right\}, \end{aligned} \quad (15)$$

$$\begin{aligned} \tau_R \frac{\partial M_m}{\partial \tau} + (\xi + \Delta_m + 3D_m^2) M_m \\ = - \left[ \xi \left( \frac{T_C}{T} - 1 \right) + 6D_m \gamma_m + 2\Pi_m \right] K_m. \end{aligned} \quad (16)$$

In accordance with our estimations<sup>29,30</sup> fluctuation dimensionless amplitude  $g = 4\pi k_B T \bar{n} \beta (\eta^{-1} - 1) / \alpha^2 e$  varies in the range from  $10^2$  to  $10^4$  for typical ferroelectric semiconductors and  $\eta(\tau, E_e) \sim (10^{-2} - 1)$ . In general case the correlator  $R^2 = -\delta\rho_S \delta n(\tau) / \bar{n}^2 = \eta(\tau) \delta\rho_S^2 / \bar{\rho}_S^2$  varies in the range (0; 1), because its amplitude is proportional to the charged defect disordering  $\delta\rho_S^2 / \bar{\rho}_S^2$  [use (3) and sample electroneutrality condition  $\bar{n} = -\bar{\rho}_S$ ]. The ratio  $\xi = -\alpha_R / \alpha \approx \alpha_{RT} T / \alpha_T (T_C - T) \sim 10^2$ , relaxation time  $\tau_R = \Gamma_R / \Gamma \sim 1$ , and dimensionless time  $\tau = -t / \alpha$ . Also dimensionless external field  $E_e = E_0 / E_C$ , built-in field  $E_m = E_i / E_C$ , and its deviation  $\delta E_m = \delta E_i / E_C$  are introduced in (7) and (8) ( $E_C = -\alpha \sqrt{-\alpha / \beta}$  is proportional to the coercive field of the perfect material with  $\delta\rho_S^2 = 0$ ). Note that  $E_m$  is almost independent over disordering  $R^2$  as caused by the smooth part of space charges  $\delta n$ , whereas  $\delta E_m$  is proportional to the defect disordering  $R^2$ , namely,  $\delta E_m \sim (\eta^{-1} - 1) R^2$  in our model [see Figs 2 and 3 and (3)].

Hereinafter we discuss only the system response near the equilibrium states, e.g., for the harmonic applied field  $E_0(t) = E_a \sin(\omega t)$  the dimensionless frequency  $w = -\Gamma \omega / \alpha$  should be smaller than unity. Additionally we assume that the series  $\eta(\tau, E_e) = \eta_0 + \sum_{i=1}^{\infty} \eta_i(w, E_a) \sin(mw\tau)$  quickly converges and  $\eta_0 \gg |\eta_i|$ , so we can substitute unknown functions  $R^2(\tau)$ ,  $g(\tau)$ ,  $E_m(\tau)$ , and  $\delta E_m(\tau)$  by their stationary parts  $R_0^2$ ,  $g_0$ ,  $E_{m0}$ , and  $\delta E_{m0}$  and then omit subscript “0” for the sake of simplicity. However, we realize that it is only the first approximation, in fact, correlation  $\eta(\tau) \sim \delta\rho_S \delta n(\tau)$  should slightly decrease with external field frequency or amplitude increase. This result could be explained allowing for the fact that the dipole correlations “sluggish defect  $\delta\rho_S$  + mobile carriers  $\delta n$ ” weaken with the frequency or amplitude increase.

Thus the system (11)–(16) steady-state behavior is determined by the dimensionless built-in fields  $E_m$ ,  $\delta E_m$ , and frequency  $w$  as well as by the aforementioned parameters  $\xi$ ,  $R^2$ ,

$g$ , and ratio  $T/T_C$ . It appeared that under the conditions  $w < 1$ ,  $g \gg 1$ , and  $\xi \gg 1$ , the scaling parameter  $gR^2/\xi$  determines the loop shape. Built-in field  $E_m$  determines loop horizontal shift, whereas  $\delta E_m$  determines their vertical asymmetry. However, the visible vertical asymmetry exists only under unlikely condition  $|\delta E_m| \geq 1$ . The loop shape and position are almost independent over  $\delta E_m$  under the condition  $|\delta E_m| \ll 1$ . The loop asymmetry becomes more pronounced with  $R^2$  increasing. Within the framework of our model, possible asymmetry is the main difference between the ferroelectric loops calculated for the film in comparison with the ones considered in Ref. 29 for the bulk material.

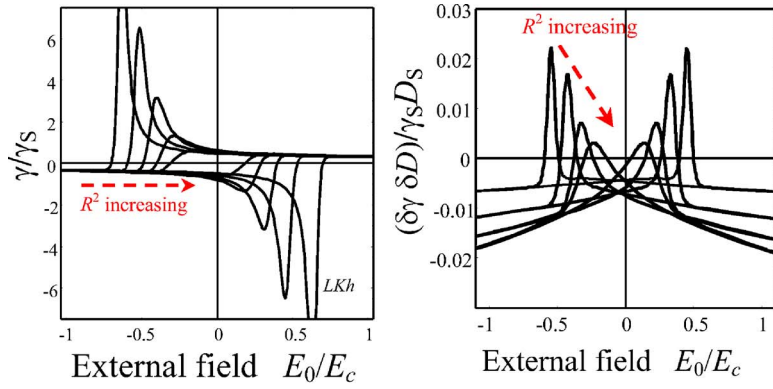
Figures 4 and 5 demonstrate the typical changes of pyroelectric and ferroelectric hysteresis loops caused by the increase of charged defect disordering (note that  $gR^2/\xi \sim \delta\rho_S^2/\bar{\rho}_S^2$ ). They prove that disorder parameters  $\overline{\delta\gamma^2} \sim \overline{\delta D^2}$  exist near the coercive field, where  $\bar{D} \rightarrow 0$ .

Let us underline that in contrast to the Landau-Khalatnikov equations describing homogeneous switching with  $\overline{\delta D^2} = 0$  near the coercive field, our coupled equations reveal *inhomogeneous* ferroelectric and pyroelectric response switching.<sup>29</sup> Namely, when the external field reaches the coercive value, the sample splits into the oppositely polarized regions, so that it is nonpolarized as a whole. Every polarized region causes displacement and pyroelectric coefficient fluctuations  $\delta\gamma$  and  $\delta D$ .

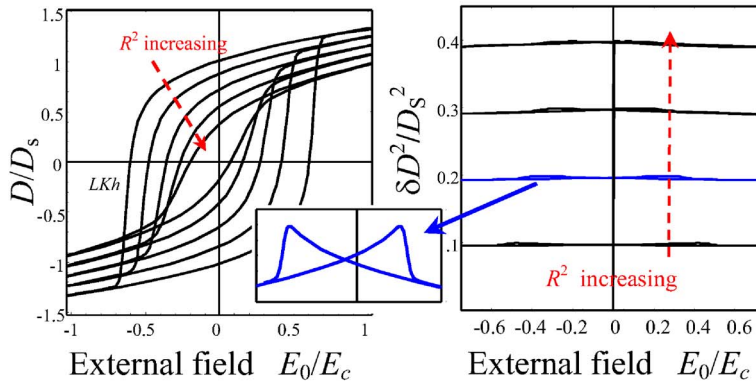
It is clear from Figs. 4 and 5 that the increase of  $gR^2/\xi$  value leads to the essential decrease and smearing of pyroelectric coefficient peaks near coercive field and to the decrease of the coercive field value (compare the Landau-Khalatnikov loops with the other ones). At  $R^2 \geq 0.5$  pyroelectric coefficient peaks near coercive field completely disappear and typical pyroelectric hysteresis loop looks like the ferroelectric one. At  $R^2 \geq 0.7$  the coercive field is much smaller than its thermodynamic value at  $R^2 = 0$ . Thus pyroelectric and ferroelectric loops become sloped, much thinner, and little lower under the increase charged defects disordering  $\delta\rho_S^2$ . This effect is similar to the well-known *square to slim transition* of the ferroelectric hysteresis loops in relaxor ferroelectrics.<sup>24</sup>

The changes of dielectric permittivity hysteresis caused by the increase of charged defect disordering are presented in Fig. 6. It is clear that disordering  $R^2$  increase shifts and smears dielectric permittivity maximum and thus leads to the degradation of the film ferroelectric and dielectric properties. Built-in field mainly shifts the hysteresis loops in the film.

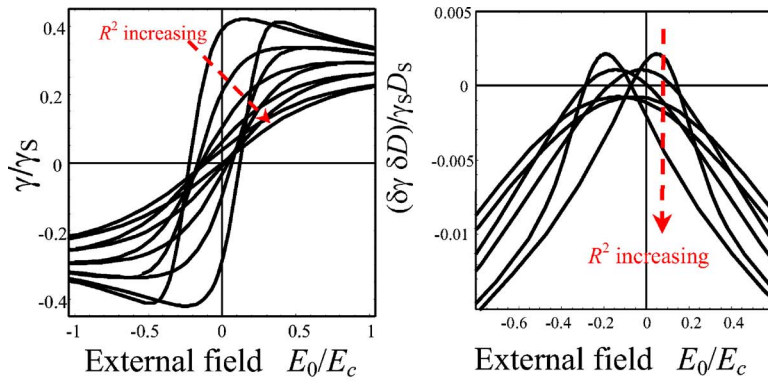
Let us underline that we do not know any experiment in which pyroelectric coefficient peaks near coercive field had been observed. Moreover, usually pyroelectric hysteresis loops in doped ferroelectrics have typical “slim” shape with coercive field values much lower than the thermodynamic one.<sup>13,14</sup> Though simplifications and approximations have been made (e.g., Refs. 3 and 4), our approach qualitatively explains available experimental results. The quantitative comparison of our numerical modeling with typical PZT and SBN-pyroelectric loops is presented in the next section.



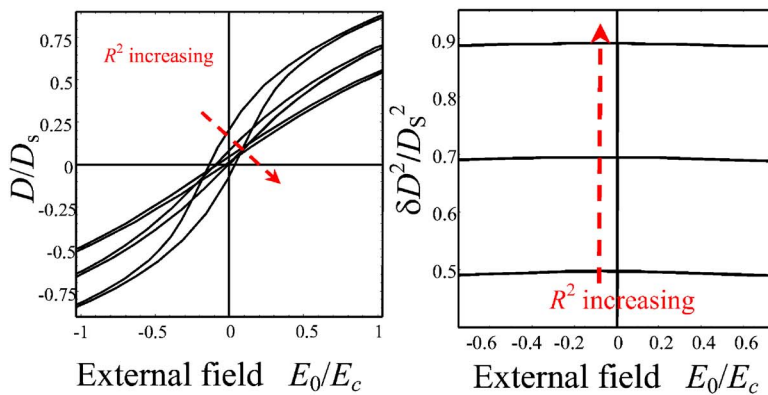
(a)



(b)



(a)



(b)

FIG. 4. Hysteresis loops of pyroelectric coefficient  $\bar{\gamma}/\gamma_S$  and its correlation  $\delta\bar{\gamma}\delta\bar{D}/(\gamma_S D_S)$  (a) and order parameter  $\bar{D}/D_S$  and disorder parameter  $\delta\bar{D}^2/D_S^2$  (b) for small values of  $R^2=0, 0.1, 0.2, 0.3,$  and  $0.4$ . Other parameters:  $g=100, \xi=100, T/T_C=0.45, w=0.025, E_m=0.05,$  and  $\delta E_m=0.5R^2$ .

FIG. 5. Hysteresis loops of pyroelectric coefficient  $\bar{\gamma}/\gamma_S$  and its correlation  $\delta\bar{\gamma}\delta\bar{D}/(\gamma_S D_S)$  (a) and order parameter  $\bar{D}/D_S$  and disorder parameter  $\delta\bar{D}^2/D_S^2$  (b) for higher values of  $R^2=0.5, 0.7,$  and  $0.9$ . Other parameters:  $g=100, \xi=100, T/T_C=0.45, w=0.025, E_m=0.05,$  and  $\delta E_m=0.5R^2$ .



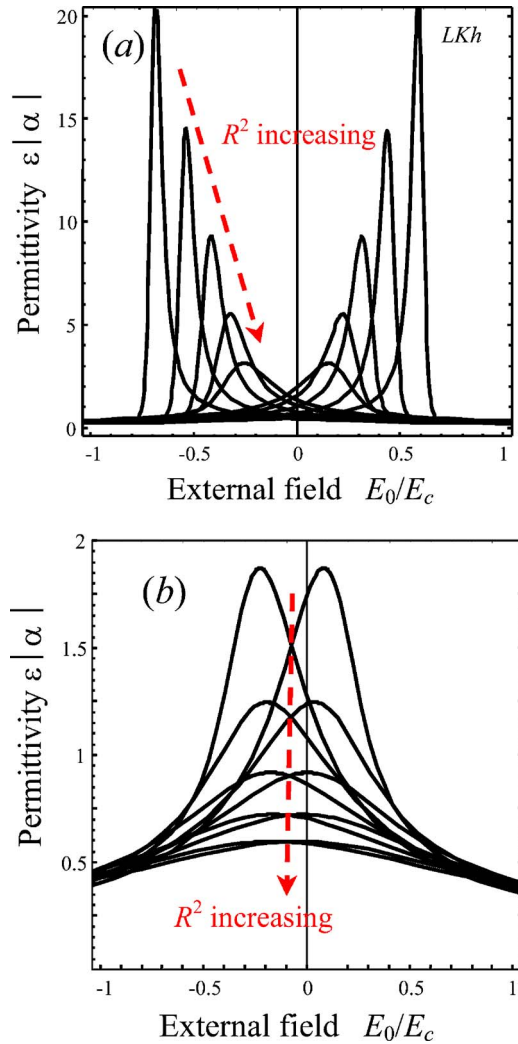


FIG. 6. Hysteresis loops of dielectric permittivity  $\bar{\epsilon}/|\alpha|$  for different  $R^2$  values:  $R^2=0, 0.1, 0.2, 0.3,$  and  $0.4$  (a) and  $R^2=0.5, 0.6, 0.7, 0.8,$  and  $0.9$  (b). Other parameters:  $g=100$ ,  $\xi=100$ ,  $T/T_c=0.45$ ,  $w=0.025$ ,  $E_m=0.05$ , and  $\delta E_m=0.5R^2$ . Calculations were performed using (A29)–(A31) derived in Appendix.

### C. Comparison with experimental results and discussion

Dopants, as well as numerous unavoidable oxygen  $O^{2-}$  vacancies, can play a role of randomly distributed charged defects in “soft” PZT. Really, it is known that low level (0.001%–1.0%) donor additives La, Nb, Nd, or Ce soften PZT dielectric and pyroelectric properties at room temperature. Ferroelectric and pyroelectric hysteresis loops have relatively high  $\gamma$  and  $D$  remnant values but reveal low coercive fields in soft PZT.<sup>9,23</sup> Usually pyroelectric hysteresis loops of PZT are rather slim and sloped even at low frequencies  $\omega \sim (0.1\text{--}10)$  Hz,<sup>9</sup> any pyroelectric coefficient maximum near the coercive field is absent.<sup>13,14</sup>

Investigated Pt–PZT–Pt/Ti–SiO<sub>2</sub>/Si structures with oriented PZT layer were manufactured by radio frequency magnetron sputtering in the system under the conditions described previously.<sup>26</sup> The sputtering target obtained by uniaxial cold pressing includes the mixture of PbO, TiO<sub>2</sub>, and ZrO<sub>2</sub> in a stoichiometric composition. The structure includes the top 150 nm Pt electrode, 1.9  $\mu\text{m}$  layer of oriented

PZT, and bottom Pt/Ti bilayer (150 nm of Pt and 10 nm of Ti) deposited onto the oxidized (350 nm of SiO<sub>2</sub>) (100)  $n$ -type Si 350  $\mu\text{m}$  substrate.

For PZT–Si-substrate structure it is necessary to design the bottom electrode, which possesses not only a stable and high enough electrical conductivity but also simultaneously prevents the interfacial reactions between electrode, PZT, and SiO<sub>2</sub> components in PZT-film and Si-substrate surroundings under rather high temperature. The layer of Ti plays an important role in limiting the diffusion of Ti in Pt/Ti intermediate bilayer through Pt layer into the PZT layer and directly into SiO<sub>2</sub> layer, and also in correction of poor adhesion of Pt layer. The annealing treatment of the Pt/TiO<sub>x</sub>/SiO<sub>2</sub>/Si-substrate structure just before PZT deposition was performed for substrate stabilization, and postannealing treatment of PZT film was performed for crystallizing the film in the polar perovskite phase. The top Pt electrode has 1 mm<sup>2</sup> area.

The pyroelectric response  $U_\pi \sim \bar{\gamma}$  of the Pt–PZT–Pt/Ti–SiO<sub>2</sub>/Si structure with oriented 2- $\mu\text{m}$ -thick PZT(46/54):Nb film was obtained with the help of modulated thermal flux method.<sup>13</sup> During the measurements quasi-static applied voltage varied in the range (–11 V, +11 V) with low frequency  $\omega \sim 0.2$  Hz; the temperature  $T$  changes with the frequency about 20 Hz. Ferroelectric and dielectric hysteresis loops are measured for the same PZT films by using the conventional Sawyer-Tower method and impedance analyzer at higher frequencies  $\omega \sim 1$  Hz. Note that a film capacity is proportional to the dielectric permittivity  $\bar{\epsilon}$  (see equations for  $\bar{\epsilon}$  in the end of Appendix). Stabilized loops (i.e., obtained after many circles) and our calculations are compared in Fig. 7.

It is clear from Fig. 7(b) that ferroelectric loop is slightly asymmetrical, i.e., built-in electric field  $E_i \neq 0$ , whereas the pyroelectric loop measured at lower frequency look almost symmetrical. Note that sometimes even stabilized loops are asymmetrical. For instance even rather thick films of disordered ferroelectric SBN grown on different substrates typically reveal shifted ferroelectric and pyroelectric loops.<sup>14</sup> The pyroelectric loop of 6- $\mu\text{m}$ -thick SBN-0.5 film on Si–SiO<sub>2</sub> substrate is compared with our calculations in Fig. 8.

It is clear from Figs. 7 and 8 that our model both qualitatively and quantitatively describes pyroelectric hysteresis loops in thick soft PZT and relaxor SBN films. Our modeling of ferroelectric and dielectric hysteresis loops was performed earlier (see, e.g., Ref. 29). Thus, despite used simplifications and approximations may require more background, verification, and/or specification, the modeling based on the coupled equations [(5)–(10)] gives realistic coercive field values and typical pyroelectric hysteresis loop shape, in contrast to the Landau-Khalatnikov approach, that describes the homogeneous pyroelectric coefficient switching. Taking into account that the inhomogeneous switching of spontaneous polarization and pyroelectric response occurs in the inhomogeneous and disordered ferroelectrics semiconductors, the proposed coupled equations can be more relevant for the phenomeno-

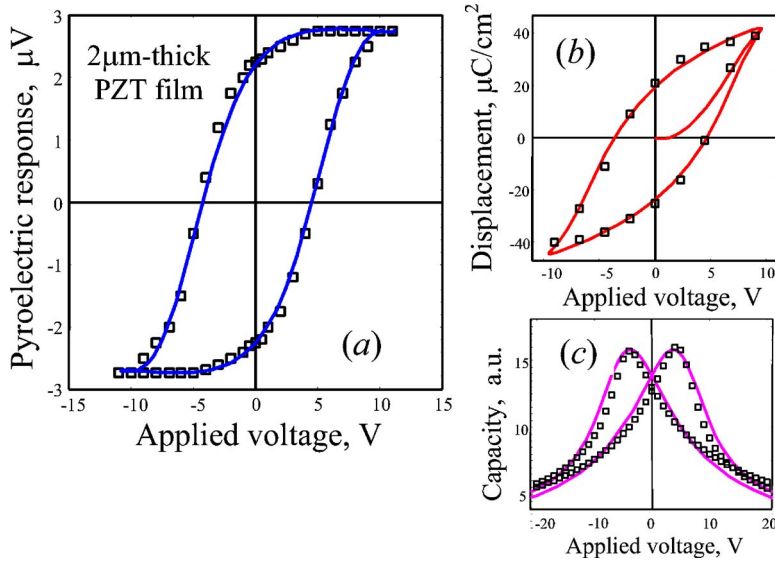


FIG. 7. Typical pyroelectric (a) and ferroelectric (b) loops of 2- $\mu\text{m}$ -thick PZT(46/54):Nb film in on Ti-SiO<sub>2</sub>/Si substrate. Squares are experimental data measured at  $T=300$  K; solid curves are our calculation with the fitting parameters  $R^2=0.5$ ,  $g=100$ ,  $\xi=100$ , and  $E_m=-0.03$  and  $w=0.11$  (a),  $w=0.6$  (b), and  $w=0.4$  (c). All other parameters correspond to the ones for perfect PZT(46/54) solid solution (Ref. 9).

logical description of their polar and pyroelectric properties than the models based on the Landau-Khalatnikov phenomenology.

## APPENDIX

We assume that the period of the changing external field is small enough for the validity of the quasistatic approximation  $\text{rot } \mathbf{E}=0$  and  $\text{rot } \mathbf{H}=0$ . Thus, Maxwell's equations for the quasistatic electric field  $\mathbf{E}$  and displacement  $\mathbf{D}$  have the form

$$\text{div } \mathbf{D} = 4\pi[\rho_S(\mathbf{r}) + n(\mathbf{r}, t)],$$

$$\frac{\partial \mathbf{D}}{\partial t} + 4\pi \mathbf{j}_c = 0. \quad (\text{A1})$$

They have to be supplemented by the material expression for current charge density:

$$\mathbf{j}_c = \sum_{\rho_m=\rho_S, n} (\mu_m \rho_m \mathbf{E} - \kappa_m \text{grad } \rho_m) \approx \mu n \mathbf{E} - \kappa \text{grad } n. \quad (\text{A2})$$

Here  $\mathbf{j}_c$  is the macroscopic free-carrier current and  $\rho_s(\mathbf{r})$  is the fluctuating charge density of the sluggish defects. One could take into account only electron mobility  $\mu$  and diffusion coefficient  $\kappa$ , allowing for the defect sluggishness. Hereinafter  $n < 0$ ,  $\mu < 0$ , and  $\kappa > 0$ . As the equation of state, we use the Landau-Khalatnikov equation for the displacement  $z$ -component relaxation but take into account the charged defects and correlation effects (i.e.,  $\partial^2 D_z / \partial \mathbf{r}^2 \neq 0$ ):

$$\Gamma \frac{\partial D_z}{\partial t} + \alpha D_z + \beta D_z^3 - \lambda \frac{\partial^2 D_z}{\partial \mathbf{r}^2} = E_z. \quad (\text{A3})$$

Parameter  $\Gamma > 0$  is the kinetic coefficient and  $\alpha < 0$ ,  $\beta > 0$ , and  $\lambda > 0$  are material parameters of the hypothetical pure (free of defects) sample.

The Debye screening radius  $R_D = \sqrt{\kappa / 4\pi n \mu} \approx \sqrt{|k_B T^* / 4\pi n e|}$  in accordance with the Einstein relation  $\mu / \kappa \approx e / k_B T^*$  (electron charge  $e < 0$ ).<sup>33,34</sup> Hereafter we suppose that homogeneous external field  $E_0(t)$  is applied along

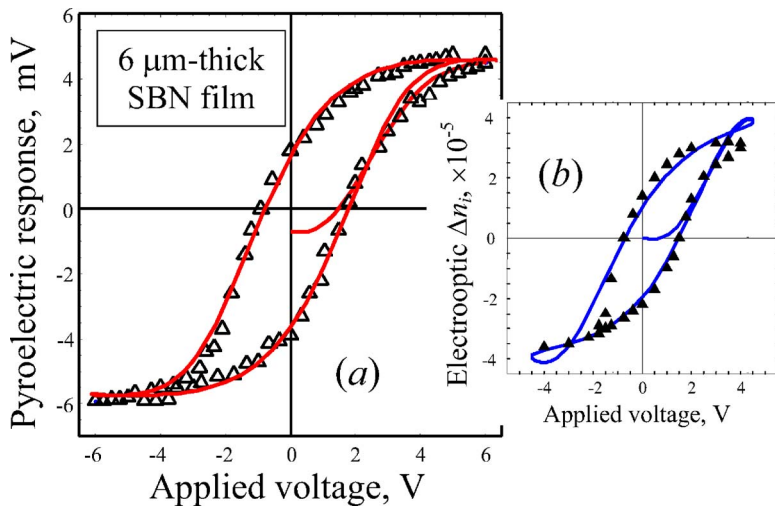


FIG. 8. Pyroelectric response  $U_\pi \sim \bar{\gamma}$  (a) and electro-optic modulation  $\Delta n_i \sim \bar{\epsilon} \bar{D}$  [(b) at  $\omega \sim 1$  kHz] obtained for 6- $\mu\text{m}$ -thick SBN-0.5 film on Si-SiO<sub>2</sub> substrate. Squares are experimental data measured by Kostsov *et al.* (Ref. 14) at room temperature; solid curve is our calculation with the fitting parameters  $R^2=0.58$ ,  $g=100$ ,  $\xi=100$ , and  $E_m=-0.013$  and  $w=0.08$  (a) and  $w=0.2$  (b). All other parameters correspond to the ones for perfect SBN-0.5 (Ref. 1).

the polar  $z$  axis. The film occupies the region  $-l/2 \leq z \leq l/2$ . We suppose that the potentials of electrodes are given, so that the inner field satisfies the condition

$$\frac{1}{l} \int_{-l/2}^{l/2} E_z(\mathbf{r}, t) dz = E_0(t). \quad (\text{A4})$$

Hereinafter we introduce the representation

$$\begin{aligned} \mathbf{D}(\mathbf{r}, t) &= \mathbf{e}_z \overline{D(t)} + \delta \mathbf{D}(\mathbf{r}, t), & \mathbf{E}(\mathbf{r}, t) &= \mathbf{e}_z E_0(t) + \delta \mathbf{E}(\mathbf{r}, t), \\ \rho_S(\mathbf{r}) &= \bar{\rho}_S + \delta \rho_S(\mathbf{r}), & n(\mathbf{r}, t) &= \bar{n} + \delta n(\mathbf{r}, t). \end{aligned} \quad (\text{A5})$$

An overbar designates the averaging of the function  $f$  over the film volume  $V$ :  $\bar{f}(t) = (1/V) \int_V f(\mathbf{r}, t) d\mathbf{r}$ . By definition  $\delta f(\mathbf{r}, t) = 0$ , where  $f = \{n, \rho_S, E, D, \dots\}$ . Here  $\mathbf{e}_z$  is the unit vector directed along the  $z$  axis,  $\bar{E}$  is the applied uniform field  $E_0(t)$ , and  $\bar{E}_{x,y} = 0$ .

The spatial distribution of the deviations  $\delta f(\mathbf{r}, t)$  consists of the part caused by spontaneous displacement screening,<sup>1,15</sup> space-charged layers localized in the ultrathin screening regions near the electrodes/substrate,<sup>15,16</sup> and the one caused by microscopic modulation  $\delta \rho_S$  with quasihomogeneous spatial distribution. For the micrometer-thick sample the averaging over sample volume is equivalent to the statistical averaging with homogeneous distribution function. Using the distribution function properties under the averaging, we obtained from (A1)–(A3) the equations for the average quantities and their fluctuations:

$$\bar{n} = -\bar{\rho}_S, \quad (\text{A6})$$

$$\text{div}(\delta \mathbf{D}) = 4\pi(\delta n + \delta \rho_S), \quad (\text{A7})$$

$$\mu \bar{n} E_0 + \mu \overline{\delta n \delta E_z} + \frac{\partial \bar{D}(t)}{\partial t} \frac{1}{4\pi} = 0, \quad \mu \overline{\delta n \delta E_{x,y}} = 0, \quad (\text{A8})$$

$$\begin{aligned} \mu(\delta n E_0 \mathbf{e}_z + \bar{n} \delta \mathbf{E}) + \mu(\delta n \delta \mathbf{E} - \overline{\delta n \delta \mathbf{E}}) - \kappa \text{grad } \delta n \\ + \frac{1}{4\pi} \frac{\partial}{\partial t} \delta \mathbf{D} = 0, \end{aligned} \quad (\text{A9})$$

$$\Gamma \frac{\partial \bar{D}}{\partial t} + (\alpha + 3\beta \overline{\delta D^2}) \bar{D} + \beta \bar{D}^3 - \lambda \frac{\partial^2 \bar{D}}{\partial \mathbf{r}^2} = E_0(t), \quad (\text{A10})$$

$$\begin{aligned} \Gamma \frac{\partial}{\partial t} \delta D + (\alpha + 3\beta \overline{\delta D^2}) \delta D + 3\beta \bar{D}(\delta D^2 - \overline{\delta D^2}) + \beta \delta D^3 \\ - \lambda \frac{\partial^2 \delta D}{\partial \mathbf{r}^2} = \delta E_z. \end{aligned} \quad (\text{A11})$$

Note that the absence of the space charge average density  $0 = \bar{n} + \bar{\rho}_S$  in (A6) means the sample electroneutrality. The term  $\mu(\delta n \delta \mathbf{E} - \overline{\delta n \delta \mathbf{E}})$  in (A8) can be interpreted as the fluctuating circular electric currents around charged defects, which do not contribute into the average macroscopic current. Also we denote  $\delta D_z \equiv \delta D$  in (A11).

The system of Eqs. (A6)–(A11) is complete, because the quantities  $\delta n$  and  $\delta \mathbf{E}$  can be expressed via the fluctuations of displacement  $\delta D$  and  $\delta \rho_S(\mathbf{r})$ , namely, in accordance with

(A7)–(A9):  $\delta n = (1/4\pi) \text{div}(\delta \mathbf{D}) - \delta \rho_S$ ,  $\overline{\delta n \delta E_z} = -\bar{n} E_0 - (\partial/\partial t) \times [\bar{D}(t)/4\pi\mu]$ , and  $\delta E_z = -(1/4\pi\mu\bar{n})(\partial/\partial t) \delta D - (\delta n/\bar{n}) E_0(t) + (\kappa/\mu\bar{n})(\partial/\partial z) \delta n + (\delta n \delta E_z - \overline{\delta n \delta E_z})/\bar{n}$ . Then the spatial distribution and temporal evolution of the displacement  $D(\mathbf{r}, t)$  are determined by the nonlinear system (A10) and (A11) allowing for the fact that (A11) could be rewritten in the form

$$\begin{aligned} \left( \Gamma + \frac{1}{4\pi\mu\bar{n}} \right) \frac{\partial}{\partial t} \delta D + (\alpha + 3\beta \overline{\delta D^2}) \delta D + 3\beta \bar{D}(\delta D^2 - \overline{\delta D^2}) \\ + \beta \delta D^3 - \left( \lambda + \frac{\kappa}{4\pi\mu\bar{n}} \right) \frac{\partial^2 \delta D}{\partial \mathbf{r}^2} \\ = - \frac{\kappa}{\mu\bar{n}} \frac{\partial \delta \rho_S}{\partial z} - \frac{E_0(t)}{\bar{n}} \delta n - \frac{\delta n \delta E_z - \overline{\delta n \delta E_z}}{\bar{n}}. \end{aligned} \quad (\text{A12})$$

However, in our opinion, only the adopted for the stochastic differential equation implicit numerical schemes can be used in order to obtain the numerical solutions of (A6)–(A11) supplemented by the appropriate distributions of fluctuations  $\delta \rho_S(\mathbf{r})$  and boundary conditions for  $\delta D(z = \pm l/2)$ , which is beyond the scope of this paper. Similar problems for the ferroelectric ideal insulators were considered in details earlier (see, e.g., Refs. 40 and 41). Therefore, hereinafter we consider only the average characteristics.

The coupled equations for  $\overline{\delta D^2}$  and  $\overline{\delta D \delta \rho_S}$  could be obtained directly from (A12) after multiplying over  $\delta D$  or  $\delta \rho_S$  and averaging. Along with (A10) they have the form

$$\Gamma \frac{\partial \bar{D}}{\partial t} + (\alpha + 3\beta \overline{\delta D^2}) \bar{D} + \beta \bar{D}^3 = \lambda \frac{\partial^2 \bar{D}}{\partial \mathbf{r}^2} + E_0(t), \quad (\text{A13})$$

$$\begin{aligned} \left( \Gamma + \frac{1}{4\pi\mu\bar{n}} \right) \frac{\partial}{\partial t} \overline{\delta D^2} + [\alpha + 3\beta \overline{\delta D^2}(t)] \overline{\delta D^2} + \beta \overline{\delta D^4} \\ + 3\beta \bar{D} \overline{\delta D^3} = \left( \lambda + \frac{\kappa}{4\pi\mu\bar{n}} \right) \overline{\delta D \frac{\partial^2 \delta D}{\partial \mathbf{r}^2}} - \frac{\kappa}{\mu\bar{n}} \overline{\delta D \frac{\partial \delta \rho_S}{\partial z}} \\ - E_0 \frac{\overline{\delta D \delta n}}{\bar{n}} - \overline{\delta D \frac{\delta n \delta E_z - \overline{\delta n \delta E_z}}{\bar{n}}} \end{aligned} \quad (\text{A14})$$

$$\begin{aligned} \left( \Gamma + \frac{1}{4\pi\mu\bar{n}} \right) \frac{\partial}{\partial t} \overline{\delta D \delta \rho_S} + [\alpha + 3\beta \overline{\delta D^2}(t)] \overline{\delta D \delta \rho_S} \\ + \beta \overline{\delta D^3 \delta \rho_S} + 3\beta \bar{D} \overline{\delta D^2 \delta \rho_S} = \left( \lambda + \frac{\kappa}{4\pi\mu\bar{n}} \right) \overline{\delta \rho_S \frac{\partial^2 \delta D}{\partial \mathbf{r}^2}} \\ - \frac{\kappa}{2\mu\bar{n}} \overline{\frac{\partial \delta \rho_S^2}{\partial z}} - E_0 \frac{\overline{\delta \rho_S \delta n}}{\bar{n}} - \overline{\delta \rho_S \frac{\delta n \delta E_z - \overline{\delta n \delta E_z}}{\bar{n}}}. \end{aligned} \quad (\text{A15})$$

Using the Bogolubov method,<sup>42</sup> the fourth and the third power correlations in (A14) and (A15) could be approximated as

$$\overline{\delta D^4} \approx (\overline{\delta D^2})^2, \quad \overline{\delta D^3} \approx 0,$$

$$\overline{\delta D(\delta n \delta \mathbf{E} - \overline{\delta n \delta \mathbf{E}})} \approx \overline{\delta D(\delta n \delta \mathbf{E} - \overline{\delta n \delta \mathbf{E}})} = 0,$$

$$\overline{\delta D^3 \delta \rho_S} \approx \overline{\delta D^2 \delta D \delta \rho_S}, \quad \overline{\delta D^2 \delta \rho_S} \approx 0, \\ \overline{\delta \rho_S (\delta n \delta \mathbf{E} - \delta n \delta \mathbf{E})} \approx \overline{\delta \rho_S (\delta n \delta \mathbf{E} - \delta n \delta \mathbf{E})} = 0. \quad (\text{A16})$$

The expressions for other correlations in (A13) and (A14) were derived in Ref. 29 for the bulk sample. In the present paper we approximate them for a finite film with thickness  $l$  with the quasihomogeneous distribution of charged defects [i.e.,  $\overline{\delta \rho_S^2} = \text{const}$ ,  $\overline{(\delta \rho_S)_{x,y}} = 0$  for every  $z$  from the region  $-l/2 \leq z \leq l/2$ ].

In accordance with (A7) built-in field  $E_i \equiv \lambda \overline{\partial^2 \delta D / \partial \mathbf{r}^2}$  acquires the form

$$E_i = \lambda \overline{\left( \frac{\partial \delta D}{\partial z} \right)_{x,y}} = \frac{4\pi\lambda}{l} \overline{(\delta n + \delta \rho_S)_{x,y}} \Big|_{-l/2}^{+l/2} \\ \approx \frac{4\pi\lambda}{l} \overline{(\delta n)_{x,y}} \Big|_{-l/2}^{+l/2}. \quad (\text{A17})$$

For a finite film  $E_i$  is induced by the space charge layers accommodated near the nonequivalent boundaries  $z = \pm l/2$  of examined heterostructure [ $\overline{\delta n(z \approx \pm l/2)_{x,y}} \neq \overline{\delta n(z \approx -l/2)_{x,y}} \neq 0$ ].

Let us estimate the averaged gradient term correlations  $\overline{\delta D (\partial^2 \delta D / \partial \mathbf{r}^2)}$  and  $\overline{\delta \rho_S (\partial^2 \delta D / \partial \mathbf{r}^2)}$  using the Fourier representation of their complex amplitudes  $\delta \tilde{D}(\mathbf{r}, t) = \text{Re}[\delta D(\mathbf{r}, t)]$  and  $\delta \tilde{\rho}_S(\mathbf{r}, t) = \text{Re}[\delta \rho_S(\mathbf{r}, t)]$ , where

$$\delta \tilde{D}(\mathbf{r}, t) = \frac{1}{4\pi^2} \sum_{m=1}^{\infty} \int_{-\infty}^{\infty} dk_x dk_y C_m(k_x, k_y, t) \\ \times \exp \left\{ i \left[ k_x x + k_y y + \frac{2\pi m}{l} z \right] \right\}$$

and

$$\delta \tilde{\rho}_S(\mathbf{r}) = \frac{1}{4\pi^2} \sum_{m=1}^{\infty} \int_{-\infty}^{\infty} dk_x dk_y P_m(k_x, k_y) \\ \times \exp \left\{ i \left[ k_x x + k_y y + \frac{2\pi m}{l} z \right] \right\}.$$

Using delta-function representation, we obtained that

$$|\delta \tilde{D}(\mathbf{r}, t)|^2 = \sum_{m=1}^{\infty} \int_{-\infty}^{\infty} \frac{dk_x dk_y}{4\pi^2} |C_m(k_x, k_y, t)|^2, \\ \overline{\delta \tilde{D}^* \frac{\partial^2 \delta \tilde{D}}{\partial \mathbf{r}^2}} = - \sum_{m=1}^{\infty} \int_{-\infty}^{\infty} \frac{dk_x dk_y}{4\pi^2} |C_m(k_x, k_y, t)|^2 k_m^2(k_x, k_y),$$

and

$$\overline{\delta \tilde{\rho}_S^* \frac{\partial^2 \delta \tilde{D}}{\partial \mathbf{r}^2}} = - \sum_{m=1}^{\infty} \int_{-\infty}^{\infty} \frac{dk_x dk_y}{4\pi^2} P_m^* C_m k_m^2(k_x, k_y),$$

here  $k_m^2 = k_x^2 + k_y^2 + 4\pi^2 m^2 / l^2$ . Under the conditions  $d \ll l$  and  $d \ll \lambda$ , the fluctuation spatial spectra  $|C_m(k_x, k_y, t)|^2$  and  $|P_m(k_x, k_y)|^2$  have well localized maximum at wave vector  $|k_m| \approx 2\pi/d$  (one-dimensional case is depicted in Fig. 3). Thus in accordance with the Laplace integration method and

Lagrange theorem about the mean point, one obtains that

$$\overline{\delta D \frac{\partial^2 \delta D}{\partial \mathbf{r}^2}} \approx - \frac{1}{d^2} \overline{\delta D^2}, \quad \overline{\delta \rho_S \frac{\partial^2 \delta D}{\partial \mathbf{r}^2}} \approx - \frac{1}{d^2} \overline{\delta \rho_S \delta D}. \quad (\text{A18})$$

When using integration over parts and equality  $\delta n = (1/4\pi) \text{div}(\delta \mathbf{D}) - \delta \rho_S$ , we transformed the terms

$$\frac{\kappa}{\mu \bar{n}} \overline{\left( \delta D \frac{\partial}{\partial z} \delta \rho_S \right)} = \frac{\kappa}{\mu \bar{n} l} \overline{(\delta D \delta \rho_S)_{x,y}} \Big|_{-l/2}^{+l/2} \\ - \frac{4\pi\kappa}{\mu \bar{n}} \overline{\delta \rho_S (\delta \rho_S + \delta n)} \\ \approx - \frac{4\pi\kappa}{\mu \bar{n}} \overline{\delta \rho_S (\delta \rho_S + \delta n)}, \quad (\text{A19})$$

$$- E_0(t) \frac{\overline{\delta D \delta n}}{\bar{n}} = E_0(t) \frac{\overline{(\delta \rho_S \delta D)}}{\bar{n}} - \frac{E_0(t)}{8\pi \bar{n}} \overline{(\delta D^2)_{x,y}} \Big|_{-l/2}^{+l/2}. \quad (\text{A20})$$

Keeping in mind that the charged defect distribution is quasihomogeneous [i.e.,  $\overline{(\delta \rho_S)_{x,y}} \approx 0$  for every  $z$  from the region  $-l/2 \leq z \leq l/2$ ], we derive that

$$\frac{\kappa}{\mu \bar{n} l} \overline{(\delta D \delta \rho_S)_{x,y}} \Big|_{-l/2}^{+l/2} \approx 0, \quad \overline{\frac{\partial \delta \rho_S^2}{\partial z}} = \frac{1}{l} \overline{(\delta \rho_S^2)_{x,y}} \Big|_{-l/2}^{+l/2} \approx 0, \quad (\text{A21})$$

$$\delta E_i = \frac{\overline{(\delta D^2)_{x,y}} \Big|_{-l/2}^{+l/2}}{8\pi \bar{n}} = \frac{2\pi}{\bar{n}} \left[ \int_{z_0}^z dz (\delta n + \delta \rho_S) \right]_{x,y}^2 \Big|_{-l/2}^{+l/2} \\ \sim \frac{\overline{(\delta n + \delta \rho_S)^2}}{l}. \quad (\text{A22})$$

The constant  $z_0$  in (A22) can be determined from the boundary conditions for  $\overline{\delta D}_{x,y}$  at  $z=0$ .

Allowing for (A16)–(A22) three coupled equations (A13)–(A15) for the average displacement  $\bar{D}$ , its mean-square fluctuation  $\overline{\delta D^2}$  and correlation  $\overline{\delta D \delta \rho_S}$  acquire the form

$$\Gamma \frac{\partial \bar{D}}{\partial t} + (\alpha + 3\beta \overline{\delta D^2}) \bar{D} + \beta \bar{D}^3 = E_0(t) + E_i(l, t), \quad (\text{A23})$$

$$\frac{\Gamma_R}{2} \frac{\partial \overline{\delta D^2}}{\partial t} + (\alpha_R + 3\beta \overline{\delta D^2}) \overline{\delta D^2} + \beta (\overline{\delta D^2})^2 \\ = E_0(t) \left( \frac{\overline{\delta D \delta \rho_S}}{\bar{n}} - \delta E_i \right) + \frac{4\pi\kappa_B T}{\bar{n}e} \overline{\delta \rho_S (\delta \rho_S + \delta n)}, \quad (\text{A24})$$

$$\Gamma_R \frac{\partial \overline{\delta D \delta \rho_S}}{\partial t} + (\alpha_R + 3\beta \overline{\delta D^2} + \beta \overline{\delta D^2}) \overline{\delta D \delta \rho_S} \\ = - E_0(t) \frac{\overline{\delta \rho_S \delta n}}{\bar{n}}. \quad (\text{A25})$$

The coefficient  $\alpha$  in (A24) and (A25) is renormalized by gradient terms as  $\alpha_R = \alpha + (\lambda/d^2 + \kappa/4\pi\mu\bar{n}d^2)$ . The renormal-

ization of the Khalatnikov kinetic coefficient  $\Gamma_R \equiv \Gamma + \tau_m$  in (A24) and (A25) is connected with the free carrier relaxation with characteristic time  $\tau_m = 1/8\pi\mu\bar{n}$ .

In contrast to the system (A6)–(A11), the system (A23)–(A25) is not complete, namely, the correlation  $\overline{\delta\rho_S\delta n}$ , built-in field average value  $E_i(l, t)$ , and its fluctuation  $\delta E_i(l, t)$  are unknown. Differential equations or exact expressions for these values should be obtained from (A7)–(A11). In the general case hypothetical complete exact system for average values and all their correlations could contain infinite number of differential equations and thus is not the simpler problem than the solution of (A7)–(A11). Allowing for made approximations (A16) and (A18) we have no special reason to derive an exact system. Instead we prefer to deal with much simpler approximate system and thus to estimate/postulate the correlation  $\overline{\delta\rho_S\delta n}$  as it was demonstrated in Ref. 29 for a bulk sample. In Ref. 29 we derived that  $-\overline{\delta\rho_S\delta n}(t) \approx \eta\delta\rho_S^2$  ( $0 \leq \eta < 1$ ) at small enough external field amplitude. This result could also be applied to the film under small external electric field in comparison with microscopic ones, because each charged region  $\delta\rho_S$  is surrounded by the electrons  $\delta n$  in accordance with the Debye screening mechanism [see Fig. 2(b)], but the smooth part of charge density  $\delta n$  accommodated near the surface and related to the spontaneous displacement screening does not correlate with random charged defects distribution  $\delta\rho_S$  [see solid curves in Fig. 3(a)].

The average pyroelectric coefficient  $\bar{\gamma} = \partial\bar{D}/\partial T$  can be obtained by the differentiation of the coupled system (A23)–(A25) on the temperature  $T$ . We suppose that only the coefficient  $\alpha = -\alpha_T(T_C - T)$  essentially depends on temperature in usual form:  $\partial\alpha/\partial T = \alpha_T$ .<sup>1</sup> The temperature dependence of other coefficients  $\beta$ ,  $\lambda$ , and  $\Gamma$  could be neglected within the framework of the Landau-Ginsburg phenomenology for the second order phase transitions.<sup>1</sup> The temperature dependence  $\partial\bar{n}/\partial T$  could be neglected at temperatures  $T \gg E_a/k_B \sim 50$  K.<sup>33,34</sup> Also we neglect the temperature dependences  $\partial E_i/\partial T$  and  $\partial\delta E_i/\partial T$  allowing for the same reasons [ $E_i \sim \delta n$ ,  $\delta E_i \sim (\delta n + \delta\rho_S)^2$ ,  $\bar{n} \sim \exp(-E_a/k_B T)$ ]. In this way we obtained three coupled equations for pyroelectric coefficient  $\bar{\gamma} = \partial\bar{D}/\partial T$  and its correlation with displacement fluctuations  $\overline{\delta\gamma\delta D} = \delta D \partial\delta D/\partial T$  and charge defects density fluctuations  $\overline{\delta\gamma\delta\rho_S} = \partial\delta D \delta\rho_S/\partial T$ :

$$\Gamma \frac{\partial\bar{\gamma}}{\partial T} + (\alpha + 3\beta\overline{\delta D^2} + 3\beta\overline{\delta D^2})\bar{\gamma} = -(\alpha_T + 3\beta\overline{\delta\gamma^2})\bar{D}, \quad (\text{A26})$$

$$\begin{aligned} \Gamma_R \frac{\partial\overline{\delta\gamma\delta D}}{\partial T} + 2(\alpha_R + 2\beta\overline{\delta D^2} + 3\beta\overline{\delta D^2})\overline{\delta\gamma\delta D} \\ = \left[ E_0(t) \frac{\overline{\delta\gamma\delta\rho_S}}{\bar{n}} - (\alpha_{RT} + 6\beta\overline{\delta D}\bar{\gamma})\overline{\delta D^2} \right. \\ \left. + \frac{4\pi k_B}{\bar{n}e} \overline{\delta\rho_S(\delta\rho_S + \delta n)} \right], \quad (\text{A27}) \end{aligned}$$

$$\begin{aligned} \Gamma_R \frac{\partial\overline{\delta\gamma\delta\rho_S}}{\partial T} + (\alpha_R + \beta\overline{\delta D^2} + 3\beta\overline{\delta D^2})\overline{\delta\gamma\delta\rho_S} \\ = -(\alpha_{RT} + 2\beta\overline{\delta\gamma\delta D} + 6\beta\overline{\delta D}\bar{\gamma})\overline{\delta D\delta\rho_S}. \quad (\text{A28}) \end{aligned}$$

The system determining the dielectric permittivity  $\bar{\epsilon} = \partial\bar{D}/\partial E_0$  and its correlations  $\overline{\delta\epsilon\delta D} = \delta D \partial\delta D/\partial E_0$  and  $\overline{\delta\epsilon\delta\rho_S} = \partial\delta D \delta\rho_S/\partial E_0$  has the form

$$\Gamma \frac{\partial\bar{\epsilon}}{\partial T} + (\alpha + 3\beta\overline{\delta D^2} + 3\beta\overline{\delta D^2})\bar{\epsilon} = 1 - 6\beta\overline{\delta\epsilon\delta D}, \quad (\text{A29})$$

$$\begin{aligned} \Gamma_R \frac{\partial\overline{\delta\epsilon\delta D}}{\partial T} + 2(\alpha_R + 2\beta\overline{\delta D^2} + 3\beta\overline{\delta D^2})\overline{\delta\epsilon\delta D} \\ = -\frac{\overline{\delta D\delta\rho_S}}{\bar{\rho}_S} - E_0(t) \frac{\overline{\delta\epsilon\delta\rho_S}}{\bar{\rho}_S} - 6\beta\overline{\delta D^2}\bar{D}\bar{\epsilon}, \quad (\text{A30}) \end{aligned}$$

$$\begin{aligned} \Gamma_R \frac{\partial\overline{\delta\epsilon\delta\rho_S}}{\partial T} + (\alpha_R + \beta\overline{\delta D^2} + 3\beta\overline{\delta D^2})\overline{\delta\epsilon\delta\rho_S} \\ = \frac{\overline{\delta\rho_S\delta n}}{\bar{\rho}_S} - \beta(2\overline{\delta\epsilon\delta D} + 6\overline{\delta D}\bar{\epsilon})\overline{\delta D\delta\rho_S}. \quad (\text{A31}) \end{aligned}$$

<sup>1</sup>M. E. Lines and A. M. Glass, *Principles and Application of Ferroelectrics and Related Materials* (Clarendon, Oxford, 1977).

<sup>2</sup>S. B. Lang, *Phys. Today* **58**(8), 31 (2005).

<sup>3</sup>D. Bolten, U. Böttger, T. Schneller, M. Grossmann, O. Lohse, and R. Waser, *Integr. Ferroelectr.* **32**, 93 (2001).

<sup>4</sup>S. Aggarwai, I. G. Jenkins, B. Nagarai, C. J. Kerr, C. Cadney, R. Ramesh, G. Velasquez, L. Boyer, and J. T. Evans, Jr., *Appl. Phys. Lett.* **75**, 1787 (1999).

<sup>5</sup>G. A. Smolenskii, V. A. Isupov, and A. I. Agranovskaya, *Fiz. Tverd. Tela (S.-Peterburg)* **1**, 992 (1959).

<sup>6</sup>G. A. Samara, *J. Phys.: Condens. Matter* **15**, R367 (2003).

<sup>7</sup>Y. Gao, K. Uchino, and D. Viehland, *J. Appl. Phys.* **92**, 2094 (2002).

<sup>8</sup>J. Wang, K. H. Wong, H. L. W. Chan, and C. L. Choi, *Appl. Phys. A: Mater. Sci. Process.* **79**, 551 (2004).

<sup>9</sup>L. E. Cross, in *Ferroelectric Ceramics*, edited by N. Setter and E. L. Colla (Birkhauser, Basel, 1993).

<sup>10</sup>J. F. Scott, *Ferroelectric Memories* (Springer, Berlin, 2000).

<sup>11</sup>U. Böttger, in *Polar Oxides: Properties, Characterization, and Imaging*, edited by R. Waser, U. Böttger, and S. Tiedke (Wiley-VCH, Weinheim, 2005), pp. 11–38.

<sup>12</sup>V. M. Ishchuk, V. L. Cherginets, O. V. Demirskaya, A. V. Aslanov, Zh. I. Klitsova, T. S. Teplitskaya, and V. L. Sobolev, *Ferroelectrics* **298**, 135 (2004).

<sup>13</sup>S. L. Bravina, E. Cattani, N. V. Morozovsky, and D. Remiens, *Semicond. Phys., Quantum Electron. Optoelectron.* **7**, 263 (2004).

<sup>14</sup>E. G. Kostsov, *Ferroelectrics* **314**, 169 (2005).

<sup>15</sup>V. M. Fridkin, *Ferroelectrics Semiconductors* (Consultant Bureau, New York, 1980).

<sup>16</sup>V. B. Sandomirskii, Sh. S. Khalilov, and E. V. Chenskii, *Fiz. Tekh. Poluprovodn. (S.-Peterburg)* **16**, 440 (1982); *Ferroelectrics* **45**, 107 (1982).

<sup>17</sup>B. Meyer and D. Vanderbilt, *Phys. Rev. B* **63**, 205426 (2001).

<sup>18</sup>K. T. Li and V. Ch. Lo, *J. Appl. Phys.* **97**, 034107 (2005).

<sup>19</sup>A. Sharma, Z.-G. Ban, S. P. Alpay, and J. V. Mantese, *J. Appl. Phys.* **95**, 3618 (2004).

<sup>20</sup>A. M. Bratkovsky and A. P. Levanyuk, *Phys. Rev. Lett.* **94**, 107601 (2005).

<sup>21</sup>V. Ch. Lo, *J. Appl. Phys.* **94**, 3353 (2003).

<sup>22</sup>A. Gordon, S. Dorfman, and D. Fuks, *Philos. Mag. B* **82**, 63 (2002).

<sup>23</sup>B. Jaffe, W. R. Cook, and H. Jaffe, *Piezoelectric Ceramics* (Academic, London, 1971).

<sup>24</sup>L. E. Cross, *Ferroelectrics* **76**, 241 (1987).

<sup>25</sup>T. Tamura, K. Matsuura, H. Ashida, K. Konda, and S. Otani, *Appl. Phys. Lett.* **74**, 3395 (1999).

<sup>26</sup>T. Haccart, E. Cattani, and D. Remiens, *Semicond. Phys., Quantum Elec-*

- tron. Optoelectron. **5**, 78 (2002).
- <sup>27</sup>L. Baudry and J. Tournier, J. Appl. Phys. **97**, 024104 (2005).
- <sup>28</sup>A. N. Morozovska, E. A. Eliseev, E. Cattani, and D. Remiens, Semicond. Phys., Quantum Electron. Optoelectron. **7**, 251 (2004).
- <sup>29</sup>A. N. Morozovska and E. A. Eliseev, J. Phys.: Condens. Matter **16**, 8937 (2004); e-print cond-mat/0408647.
- <sup>30</sup>A. N. Morozovska and E. A. Eliseev, Physica B **355**, 236 (2005).
- <sup>31</sup>A. N. Morozovska and E. A. Eliseev, Phys. Status Solidi B **242**, 947 (2005).
- <sup>32</sup>A. N. Morozovska, Ferroelectrics **317**, 37 (2005).
- <sup>33</sup>B. I. Shklovskii and A. L. Efros, *Electronic Properties of Doped Semiconductors* (Springer, Berlin, 1984).
- <sup>34</sup>A. Y. Shik, *Electronic Properties of Inhomogeneous Semiconductors* (Gordon and Breach, New York, 1995).
- <sup>35</sup>D. Y. Gao, in *Advances in Mechanics and Mathematics*, edited by D. Y. Gao and R. W. Ogden (Kluwer Academic, Dordrecht, 2003), pp. 261–312.
- <sup>36</sup>J. Rodrigues Contreras, H. Kohlstedt, U. Poppe, R. Waser, and Ch. Buchal, Appl. Phys. Lett. **83**, 126 (2003).
- <sup>37</sup>M. Shimizu, S. Nakashima, K. Kaibara, H. Fujisawa, and H. Niu, Ferroelectrics **241**, 183 (2000).
- <sup>38</sup>M. Tyunina and J. Levoska, Phys. Rev. B **70**, 132105 (2004).
- <sup>39</sup>M. D. Glinchuk and A. N. Morozovska, J. Phys.: Condens. Matter **16**, 3517 (2004).
- <sup>40</sup>R. C. Miller and G. Weinreich, Phys. Rev. **117**, 1460 (1960).
- <sup>41</sup>W. Cao and L. E. Cross, Phys. Rev. B **44**, 5 (1991).
- <sup>42</sup>N. N. Bogolubov and D. V. Shirkov, *Quantum Fields* (Nauka, Moscow, 1980).